GEOPHYSICS, VOL. 65, NO. 5 (SEPTEMBER-OCTOBER 2000); P. 1402–1417, 16 FIGS., 2 TABLES.

Seismic exploration in complex terrains: A processing experience in the Southern Apennines

Alfredo P. Mazzotti*, Eusebio Stucchi*, Gian Luigi Fradelizio*, Luigi Zanzi‡, and Paolo Scandone**

ABSTRACT

We discuss a data-processing sequence adopted to reprocess a seismic line that crosses the Italian southern Apennines from the Tyrrhenian Sea to the Adriatic margin and investigate both the overthrust and foreland areas. We first determine the main causes of the very low S/N ratio in the field data and then propose a processing sequence aimed at exploiting the signal content, also making use of a priori geological knowledge of this area. Our work indicates a combination of causes for the very low quality of the seismic data. These include length of the spread (about 20 km) that is unfavorable because of the rapid variation in the near-surface geology, tectonic complexity, crooked-line acquisition, and the rough topography associated with outcropping rocks characterized by highly variable velocities.

Based on the outcome of this data analysis, we present a processing sequence driven by knowledge of the regional tectonic setting and by knowledge of the shallow subsurface geology. The main effort is in removing the large, near-surface related noise components. The low S/N ratio makes it impossible or nearly impossible to successfully apply highly sophisticated techniques such as depth migration or wave equation datuming. Thus, we used robust techniques specifically designed to solve each problem that degraded data quality. The most relevant of these techniques were the removal of bad traces where unacceptably low quality was detected by energy and frequency decay criteria; estimation and correction for static time shifts attributable to near-surface conditions; optimization of common midpoint (CMP) sorting to attenuate the deleterious effects of the crooked-line acquisition; application of a weighted stacking technique to maximize stack power and application of prestack f-x deconvolution to attenuate uncorrelated noise.

The outcome of this processing sequence is compared with the result of a more standard sequence that was previously applied to the same data and is also discussed in terms of the possible geological model it might evidence. The realization of a seismic section showing rather continuous and structured events down to 8 s which, depending on the interpretation, may be related to Moho discontinuity or to very deep sedimentary layers supports the efficacy of the processing approach we propose.

INTRODUCTION

Seismic exploration in complex terrains such as thrust belts and complex tectonic regimes is hampered by several factors that often lead to poor-quality data. Different processing approaches offer possible ways to improve the quality of the final sections in overthrust areas. Wu et al. (1998) explore the advantages of prestack migration from topography on the Husky structural data set and propose an iterative procedure where strong interaction between geophysicists and interpreters helps optimize the velocity field for prestack migration from topography. Zhu et al. (1998) claim that prestack depth migration from a horizontal datum after tomo-datuming, i.e., after prestack wave-equation datuming with near-surface velocity estimated from turning-ray tomography, produces better images than direct migration from topography. They test the procedure on real data from various complex areas, including the Husky Structural data set, and conclude that their assumption is particularly true when rough topography and strong near-surface velocity variation exist concurrently. Unfortunately, both approaches tend to be inapplicable when the S/N ratio of the

Manuscript received by the Editor May 7, 1999; revised manuscript received March 10, 2000.
*Università di Milano, Dipartimento di Scienze della Terra—Geofisica, Via Cicognara 7, 20129 Milan, Italy. E-mail: alfredo.mazzotti@unimi.it; eusebio@ibm.geofisica.unimi.it.
‡Politecnico di Milano, Dipartimento di Elettronica e Informazione, P.zza L. Da Vinci 32, 20133 Milan, Italy. E-mail: zanzi@elet.polimi.it.
**Università di Pisa, Dipartimento di Scienze della Terra, Via S. Maria 53, 56126 Pisa, Italy.

field data is very low; thus, techniques that are less noise sensitive than prestack migration are needed. This is the case of a regional seismic line that crosses the southern Apennines (Figure 1) near important hydrocarbon discoveries.

As shown in Figure 2, the structural domains investigated by this line include the main overthrust and foreland areas. Extensive hydrocarbon exploration in the foredeep basin and in the thrust belt has led to a much greater foreground knowledge of the internal architecture of the southern Apennines (see Balduzzi et al., 1982a,b; Mostardini and Merlini, 1986; Casnedi, 1988a,b; Sella et al., 1988; Casero et al., 1991; D'Andrea et al., 1993; Roure and Sassi, 1995; La Bella et al., 1996; Mattavelli et al. 1993). The backbone of the mountain chain has a deep-seated compressional duplex system—a target for oil exploration, overlain by a thick pile of rootless nappes. The buried duplex system is a stack of Mesozoic–Tertiary carbonate horses detached from a shallow-water platform realm (Apulia Platform) along Triassic evaporites. The rootless nappes consist of basin and platform Mesozoic–Tertiary sedimentary sequences overlain unconformably by Miocene–Pleistocene thrust-sheet-top deposits. Duplex breaching processes and out-of-sequence thrust propagation have contributed to produce a quite complex structural architecture (e.g., huge informal stacks within the roof units). Commercial seismic lines and well logs are a fundamental tool for deciphering Apennine structure. Nevertheless, because of the limited record length (usually 5 s TWT) of the seismic sections, the deep structures of the thrust belt are relatively unknown and critical first-order structural geometries are still unresolved. For instance, we do not know the location of the duplex-system trailing edge in the subsurface or the depth of the sole thrust in correspondence to the Tyrrhenian margin of the mountain chain. Furthermore, it is unknown whether the basement is involved in the crustal shortening or how far the undeformed Apulia crust extends beneath the thrust belt. So we designed and acquired a new regional seismic reflection line that cuts across the entire Apenninic chain to answer these questions.

The line was acquired in the framework of the CROP project (the Italian deep-crust exploration project) with the parameters illustrated in Table 1. The same line was also acquired with an explosive energy source, using the same recording spread as the Vibroseis acquisition and thus allowing a quantitative comparison of the two sources. We were assigned to reprocess the first 100 km of Vibroseis data starting from the Tyrrhenian coast to the site of Fiumara Venosa (from CMP 5–2600, Figure 1).

Rather than focus on each step of the processing, our paper emphasizes the key steps that noticeably improved data quality. Thus, we first describe the most significant problems affecting the field data and then present the adopted processing solutions.

ANALYSIS OF DATA QUALITY

To effectively define an appropriate processing strategy, we first performed a detailed analysis of the data to identify the different types of problems and noise to be addressed and attenuated by the subsequent processing phases. The data available for this analysis were

FIG. 1. Location map that refers to the area indicated in the upper frame; some CMP locations along the line are indicated.

1) the entire set of the Vibroseis and dynamite field records (stacked and correlated), observer's report, uphole data, elevation map, source testing results, and stacking chart;
2) a geological map (scale 1:25 000) detailing the lithological units; and
3) a geological cross-section coincident with the path of the seismic line.

Near-surface conditions

As shown in Figure 3, the roughness of the topography and the abrupt succession, within one spread length, of soft and hard near-surface lithologies characterize the course of the seismic line. These conditions require very careful processing steps such as static computation and velocity analysis; besides, under such circumstances, conventional muting schemes of first breaks are not applicable. Below the geological cross-section of Figure 3, we have also plotted the estimated refractor velocities computed for datum static corrections. The subweathering velocity is compared with the geology at the surface: the final velocity model shows good correspondence between lithology and velocity, resulting in optimal correlation when faults are present. Within one spread length there may be several hundred meters' difference in the elevation and more than 1000 m/s of near-surface velocity variation. These conditions severely test many of the simplifying assumptions made by conventional processing algorithms and methods.

Another consequence of the rough topography and the difficulties in accessibility for the Vibroseis trucks is the crooked-line acquisition of the seismic data. A typical example is shown in Figure 4 in the area between Albanella and Muro Lucano located on the western side of the Apennine chain. Such high tortuosity in many parts of the line causes conspicuous problems in common midpoint (CMP) sorting and degrades the seismic image, particularly at shallow times. Thus, the slalom line must be designed carefully to prevent degradation.

Incoherent noise contamination

Many Vibroseis shot gathers are dramatically contaminated by incoherent noise that appears suddenly at large offset (>4000 m). Such noise generally looks like uncorrelated noise (white in the Vibroseis band), affecting the whole trace record length. In a few cases, the noise spectrum is colored, presenting a dominating frequency between 20 and 30 Hz. In any case, both the noise power and the noise spectrum are, basically, time invariant. This noise might be from inadequate gain settings of the seismic group recorder (SGR) floating-point amplifiers and/or to other yet-to-be-determined reasons. In some cases, the occurrence in the spread of this peculiar noise coincides with the transition to hard-surface rocks. Thus, poor receiver coupling may be a concurrent factor in signal degradation, although a convincing surface-consistent pattern has been found only along some segments of the entire line. We also found that

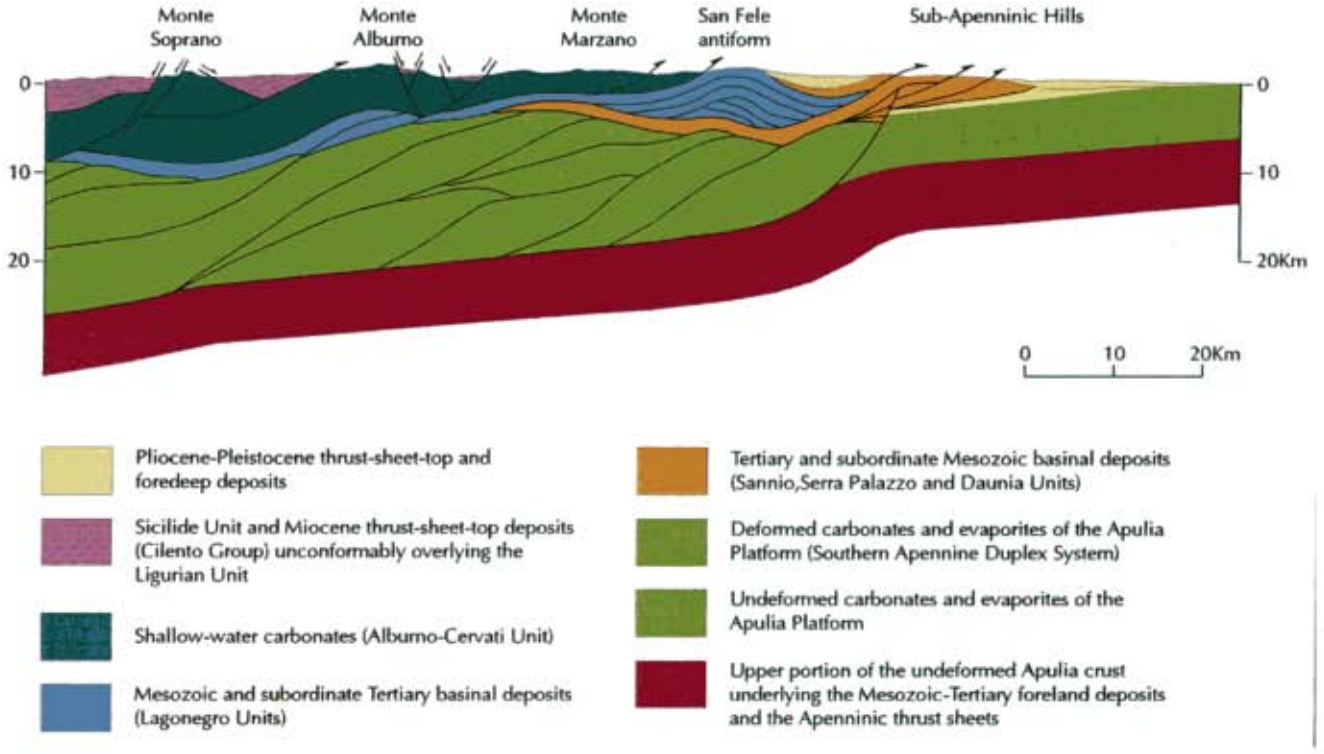

FIG. 2. Schematic geological section across the southern Apennines along the trace of the seismic line. Drilling results for hydrocarbon exploration have provided important data for constraining the base-of-Pliocene/Pleistocene isobaths in the foreland area, the internal architecture of the roof units of the thrust belt, and the top of the buried duplex system in the right half of the figure. The deep structures of the mountain chain beneath Monte Soprano and Monte Alburno, on the contrary, have never been directly explored since the maximum depth of the wells in the area slightly exceeds 4000 m. Therefore, the geological section in this part of the profile is based on the interpretation of the seismic line.

the noise content in the Vibroseis and explosive data increases significantly in areas of intense tectonic stress, which may be the cause of diffused wavefield scattering. This is particularly evident in some segments of the line, such as the one paralleling a regional normal fault that separates the Alburno carbonate massif from the Sele coastal plain (Figure 5) and in areas of overthrusting. Data of better quality were recorded in areas of lower structural complexity (Figure 6).

The poor quality of significant amounts of the data forced us to find a technique able to automatically detect traces where the quality is below a predefined threshold. To this end we used two quality indicators: average amplitude variation with time and frequency variation with time. A good trace should exhibit both amplitude decay and frequency decay with time. A bad trace is one that manifests a constant status of amplitude and frequency content with time. The rms amplitudes and frequency spectra were computed in time gates of about 0.5 s, sliding along the time axis of the data. After a few tests, suitable thresholds for rms amplitude and peak frequency variations were selected, and all the field traces were assessed for these attributes. Depending on the resulting good or bad nature of each trace, an appropriate code was inserted in a location of its header. Traces of uncertain nature, i.e., with contrasting indications from the two indicators, or with characteristics very close to the limits were flagged with a distinct code that enabled separate sorting and visual inspection to define their final status.

Figure 7 shows the percentage of bad traces with respect to the total number of traces in each common source gather. The surface lithologies at the source location are also shown. The few areas with 0% bad traces were inaccessible to the Vibroseis trucks; thus, no data were recorded. The lithology at the source location does not show a convincing relation with the occurrence of bad traces. Stronger correlations can be established with the structural complexity of the near surface. The higher occurrence of bad traces between sources 500 and 750 is associated with the position of a regional fault (see also Figure 3). The percentage of bad traces remains constantly high (40% as an approximate average) along the whole Apennine chain and starts decreasing in correspondence with the transition to less perturbed areas of the foreland basin (area of the Sub-Apenninic Hills, Figure 2). Figure 8 shows the strong dependence of data quality on source to receiver offset. At offsets greater than ±4000 m, more than 30% of the data is classified as bad.

Table 1. Acquisition parameters of the CROP 04 line.

RECORDING DATA

Record length	25 s
Sampling interval	4 ms
Channels	240
Filter L.C.	8 Hz 18 DB/OCT
Filter H.C.	88.8 Hz 48 DB/OCT

VIBROSEIS PATTERN

Number of vibrators	5
Vibrator distance	11 m
Move-up	6 m
Number of sweep/V.P.	12
Physical array length	110 m
Sweep type	linear
Sweep frequency	8 - 40 Hz
Sweep length	40 s
S.P. position	on half station
S.P. interval	80 m
Coverage	120 fold

DYNAMITE PATTERN

Total charge size	100 kg
Average hole depth	30 m
S.P. interval	variable
Coverage	4 fold

GEOPHONES

Natural frequency	10 Hz
Damping	63 %
Geophones/group	24
Pattern configuration	Linear
Geophone distance	3.5 m
Pattern length	80 m

SPREAD

Type	Split spread
Number of groups	240
Group interval	80 m
Minimum offset	360 m
Maximum offset	+/-9880 m

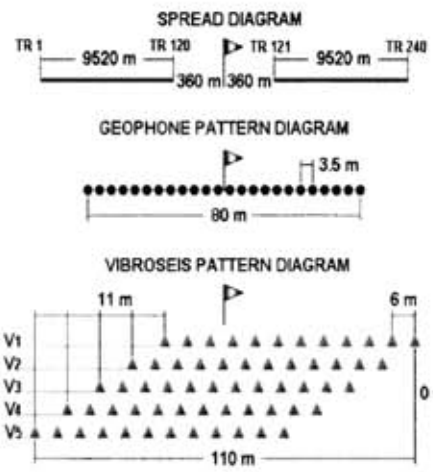

The results of this analysis were also stored in a database that can be used for further studies on possible cause-and-effect relations between data quality and seismic parameters (e.g., tortuosity of the line, type of energy source, source–receiver offset, etc.) or between data quality and geological characteristics (e.g., surface lithology at the source and/or at the receiver, local tectonic setting, etc.). The outcome of this specific study, not detailed in this paper, is useful for planning seismic acquisition in nearby areas or in zones with similar characteristics.

PROCESSING SEQUENCE

The processing sequence applied to the data is depicted in Figure 9. Instead of describing each step in sequential order, we discuss groups of processing operations, not necessarily following a data flow order. The processing steps in each group have the common aim of solving a specific problem detected in the previous data analysis. We focus our discussion on the following groups of processing steps:

1) noise attenuation operations applied throughout the whole processing sequence, but we attempted to remove the largest noise components as early as possible;
2) removal of static time shifts because of near-surface conditions, which implies the application of two different methods of refraction statics computation and a technique of surface-consistent residual statics;
3) optimization of CMP sorting and stacking to attenuate the deleterious effects of crooked-line acquisition; and
4) model-driven velocity analysis to exploit the a priori geological knowledge of the area.

For the other processing operations, not as essential to achieving the final result as those listed above, we mention only the pertinent set-up parameters (Figure 9).

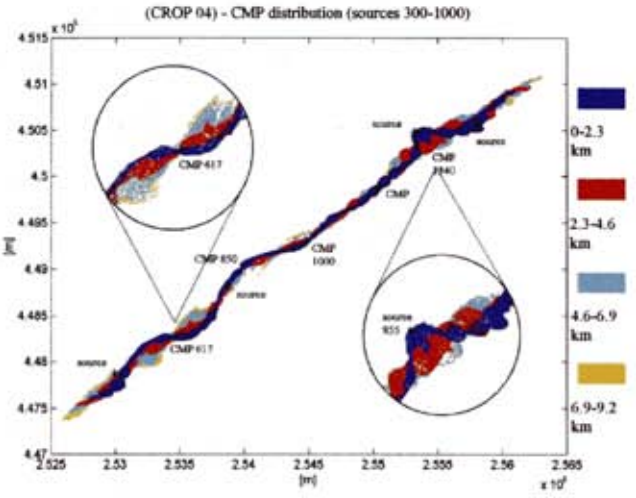

FIG. 4. An example of the crooked-line acquisition. Note the relevant dispersion of the actual CMP locations.

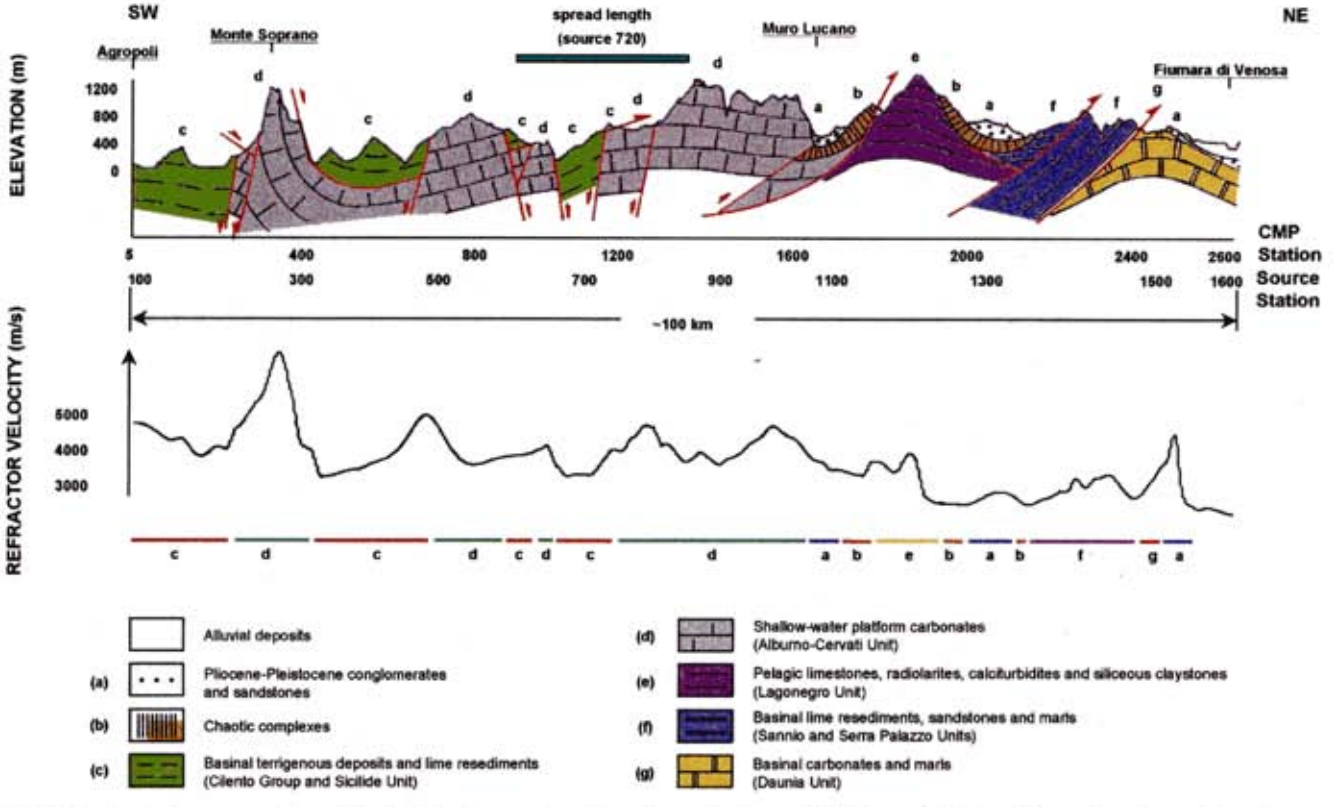

FIG. 3. Geological cross-section of the shallow formations along the seismic profile. The graph below the section shows the refractor velocity estimated for the computation of the static corrections. Note the correlation between lithology and velocity changes.

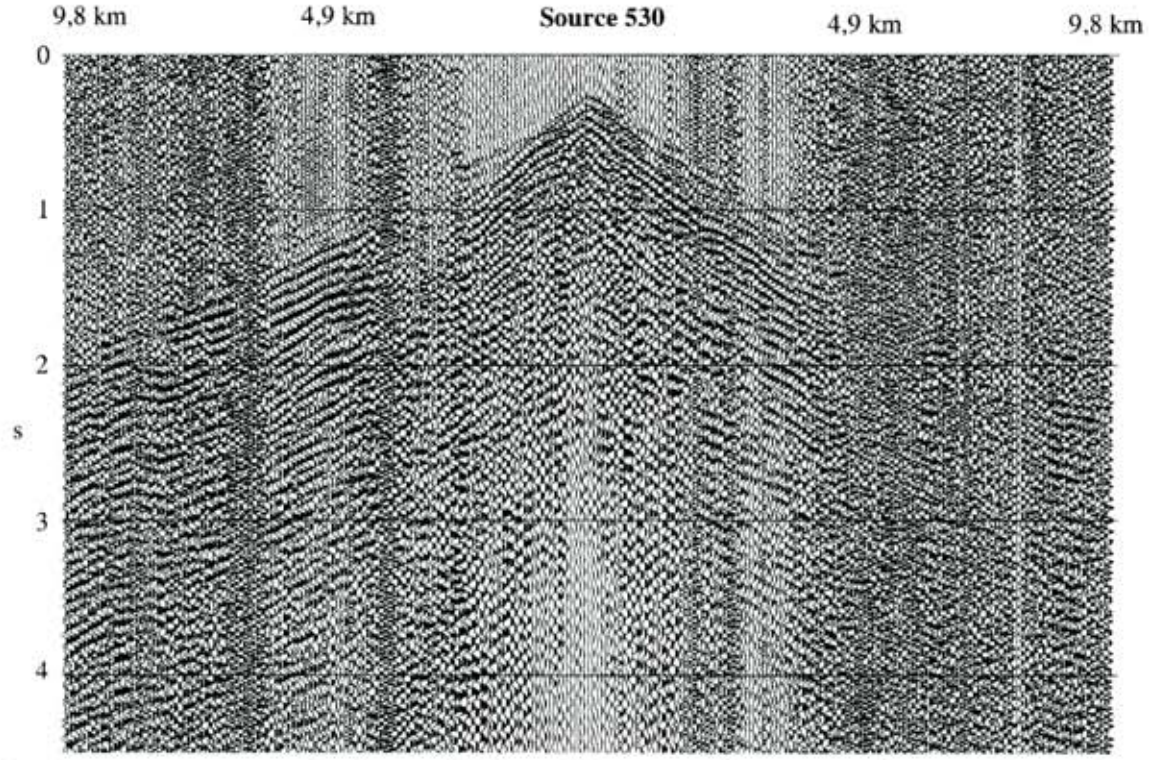

FIG. 5. A common-source gather (source 530) located in an area of intense tectonic stress and parallel to a regional fault.

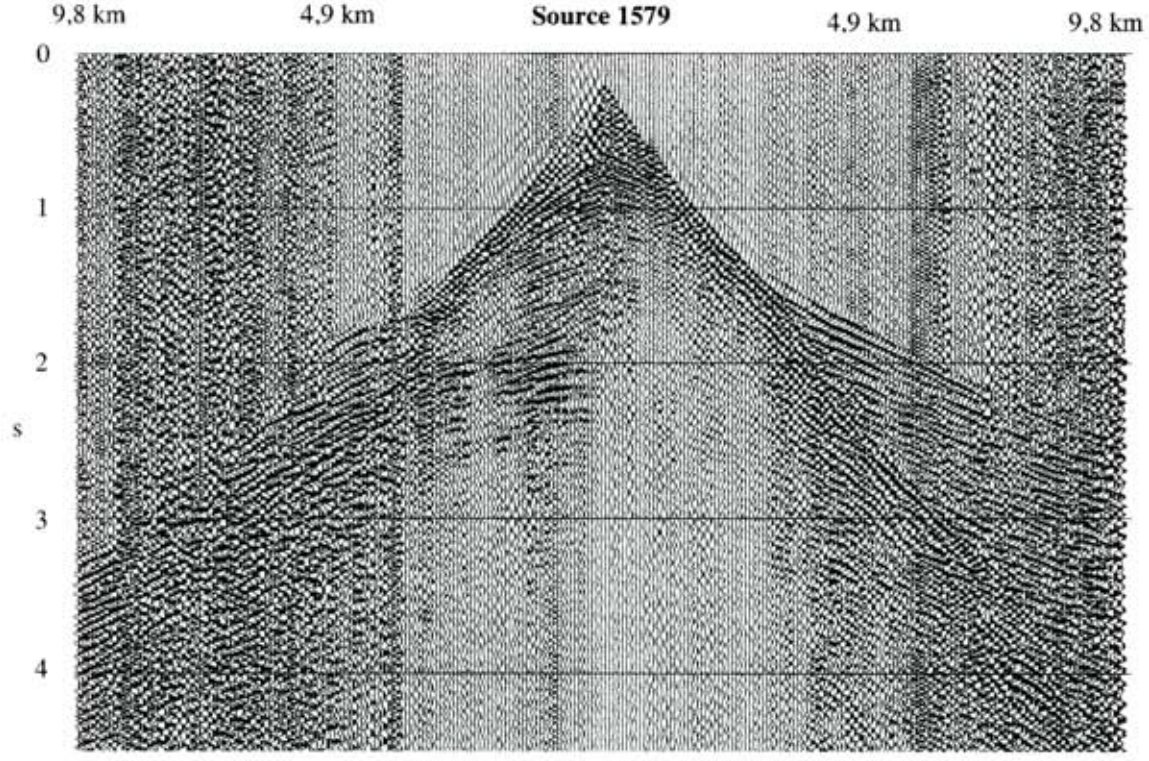

FIG. 6. A common-source gather located in the foreland area near CMP 2600 (source 1579). Data quality is better than the example in Figure 5.

Noise attenuation

Based on the trace classification conducted in the data analysis phase, the traces where the quality, as defined by the amplitude and the frequency indicators, fell below a given threshold were removed immediately from the data set. This led to rejecting about 30% of the field traces. In some areas we removed up to 70% of the data (Figure 7). This was in the zones of high tectonic disturbance and complex near-surface geology—particularly at high source–receiver offsets.

Common-offset gathers, which mimic the (time-shifted) reflector geometry of the normal-incidence single fold gather, were considered the most appropriate domain in which to apply *f-x* deconvolution. In fact, this kind of data grouping allows easy evaluation of the effectiveness of the operation and an important quality control check on the hazard of creating false events by enhancing correlated noise. The *f-x* deconvolution was performed on common-offset gathers after applying static corrections to the final (flat) datum and after filling the gaps of missing traces with null traces. An amplitude trace equalization was also applied before *f-x* deconvolution to prevent artifacts that result from unbalanced data. Offset bins of 160 m were selected so that, in nominal conditions, two traces of each source record belonged to the same common-offset gather. The total split spread active cable length (20 km) and the complexity of the area suggested sorting out the positive offsets and the negative ones; thus, we obtained a total of 120 common-offset sections. Figure 10 shows the gather at a constant offset of 3000 m before and after applying the *f-x* filter. The filter parameters (20 traces correlation in time gates of 0.4 s, six traces filter length) were carefully selected to avoid introducing excessive coherency in the data. The same parameters were adopted for

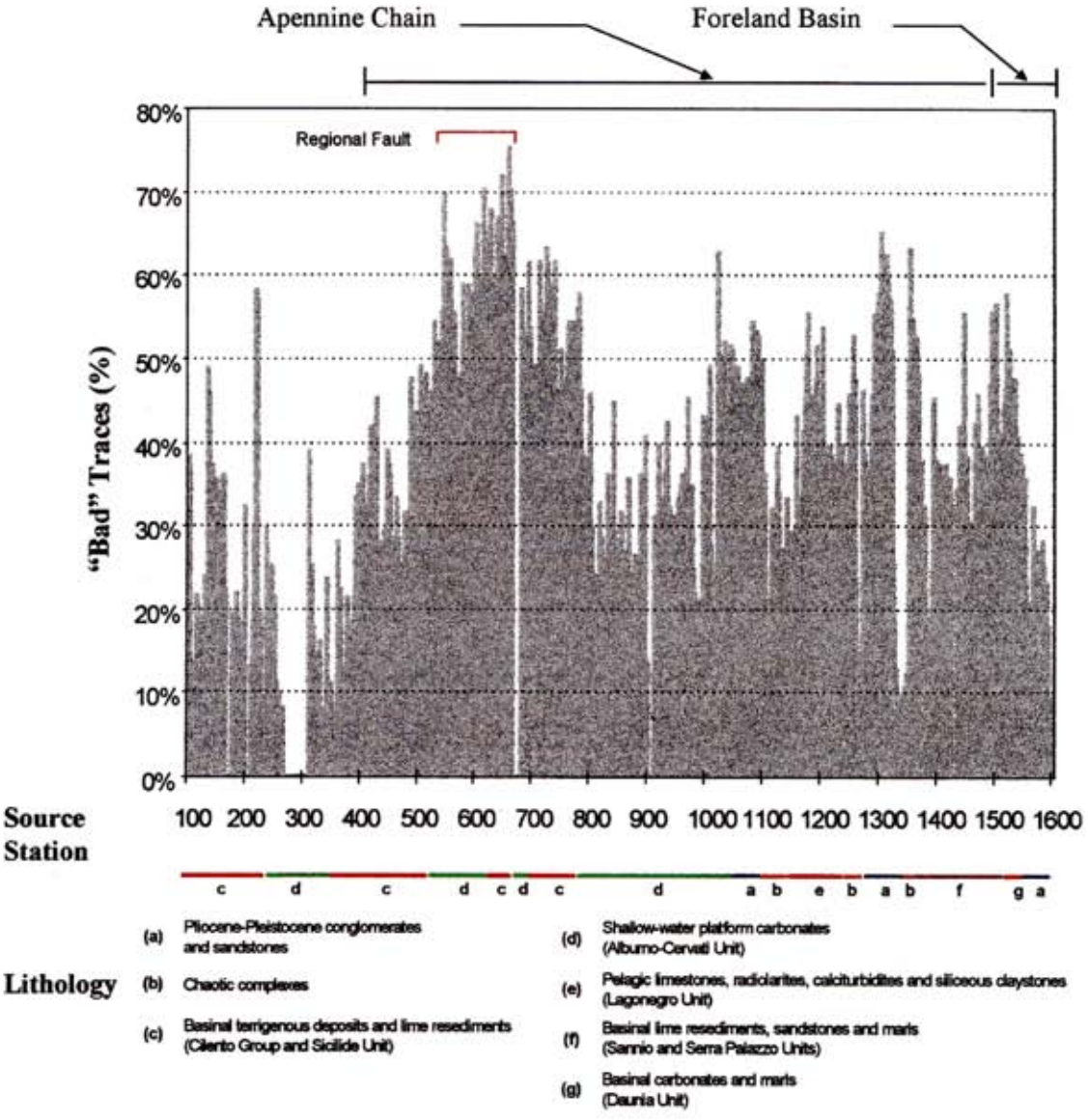

FIG. 7. Classification of Vibroseis trace quality along the profile based on amplitude and on frequency versus time indicators. The largest number of bad traces, between stations 500 and 750, corresponds to the area of the most intense tectonic deformation. Stations with null percentage of bad traces indicate the absence of Vibroseis data, not good data quality.

another *f-x* deconvolution applied on the data of the weighted stack section at the end of the proposed sequence.

Another operation effective in reducing noise is the weighted stack, where the weights are the local estimates of the S/N ratio. The computation of the local, i.e., sample-by-sample and trace-by-trace, S/N ratio of the data is carried out by means of singular value decomposition (SVD) or, alternatively, by correlating adjacent traces (Grion and Mazzotti, 1998). These weights were computed on NMO-corrected CMP gathers after final velocity analysis and residual statics application by estimating the data coherence within a small sliding time-space window. The window dimensions are three or five traces by a time length chosen to contain at least one wavelet. Figure 11 shows the original CMP (left) and the pertinent weights (right) computed with a method based on the sum of the zero lag values of the crosscorrelation between three adjacent traces and with a window time length of 112 ms. Higher weights are assigned to data samples showing a more pronounced spatial continuity, while noisy zones are penalized. These coefficients may be used directly to weight the data samples, as done in this case, or may be processed further (e.g., smoothed or gained) to produce the final stacking weights. Similar weights were also obtained with a more CPU-demanding method based on the SVD technique. Since the results were very similar, the crosscorrelation method, twice as fast as the SVD method, was preferred.

Removal of static time shifts

The computation of static corrections required a lot of manpower. First-break picking was carried out manually on both the Vibroseis and the dynamite data. First-break picking of Vibroseis data is known to be troublesome, mainly because of the precursory events that parallel the true first break. In this case the picking was made more difficult by the noise that often obscured the first breaks. To render this operation more reliable, we included the (low-fold) explosive data that show much cleaner first breaks and guided the picking in the adjacent Vibroseis gathers. Attempts to operate with two refractors were frustrated by the insufficient coverage of first breaks,

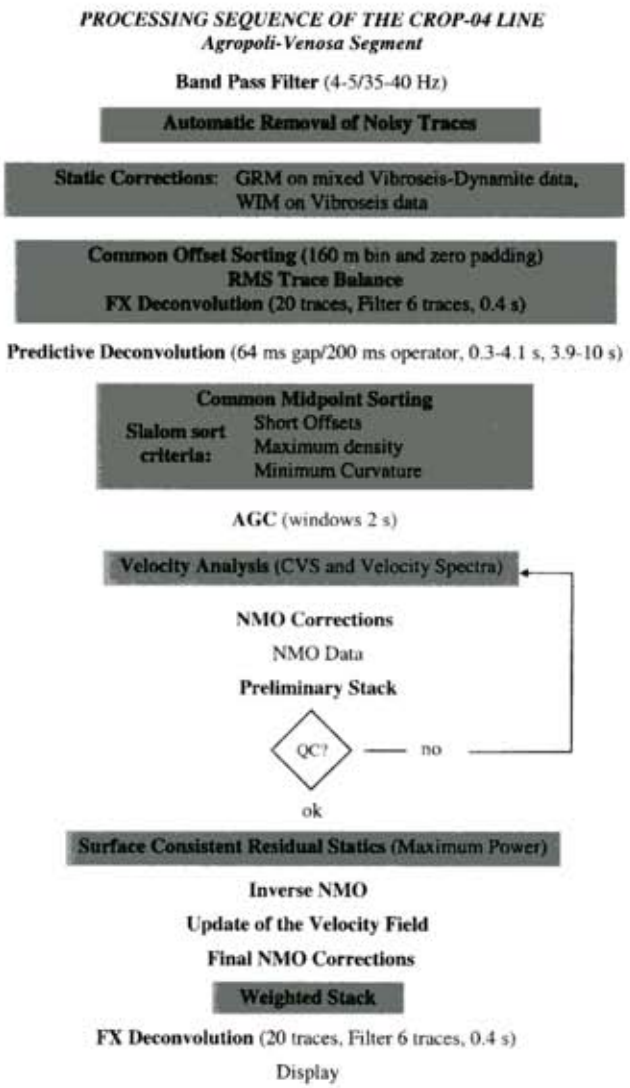

FIG. 9. Flow chart of the processing sequence. The steps marked by a shaded box are discussed in detail in the text. The relevant set-up parameters of the other steps are indicated.

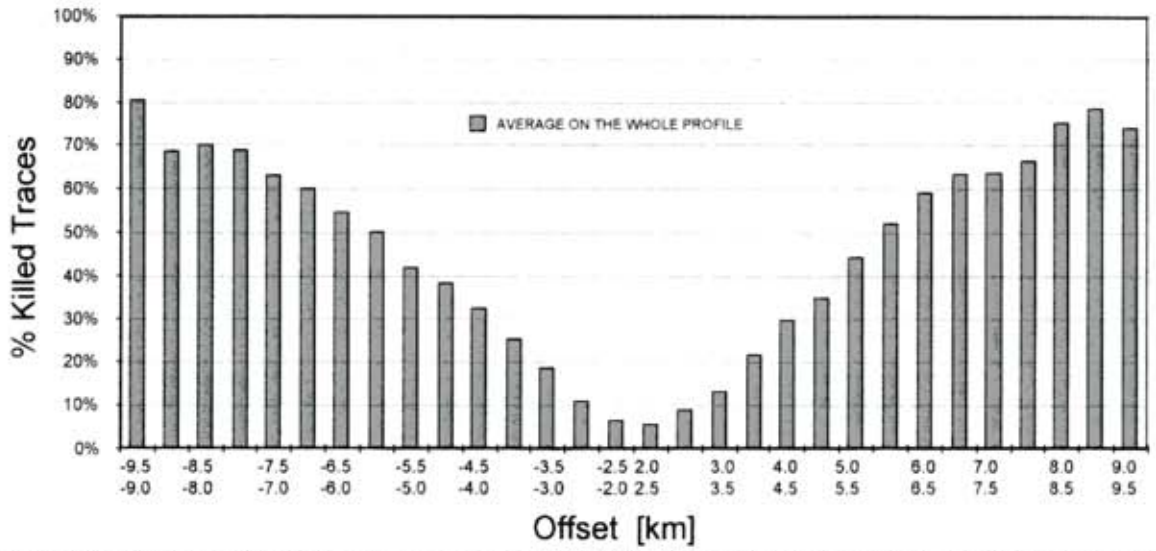

FIG. 8. Classification of Vibroseis trace quality versus source–receiver offset. The percentage of bad traces increases with increasing source–receiver offset. For offsets greater than ±4000 m, the percentage of bad traces exceeds 30%.

especially at the far offset where accurate picking was rarely possible because of noise contamination. Thus, we worked with a single refractor. On average, reliable breaks were picked up to 3000 m.

The velocity for the first layer of the model was reconstructed by interpolating the information derived from uphole times. As a consequence of the near-surface complexity and the crooked-line acquisition, the near-surface velocity–depth

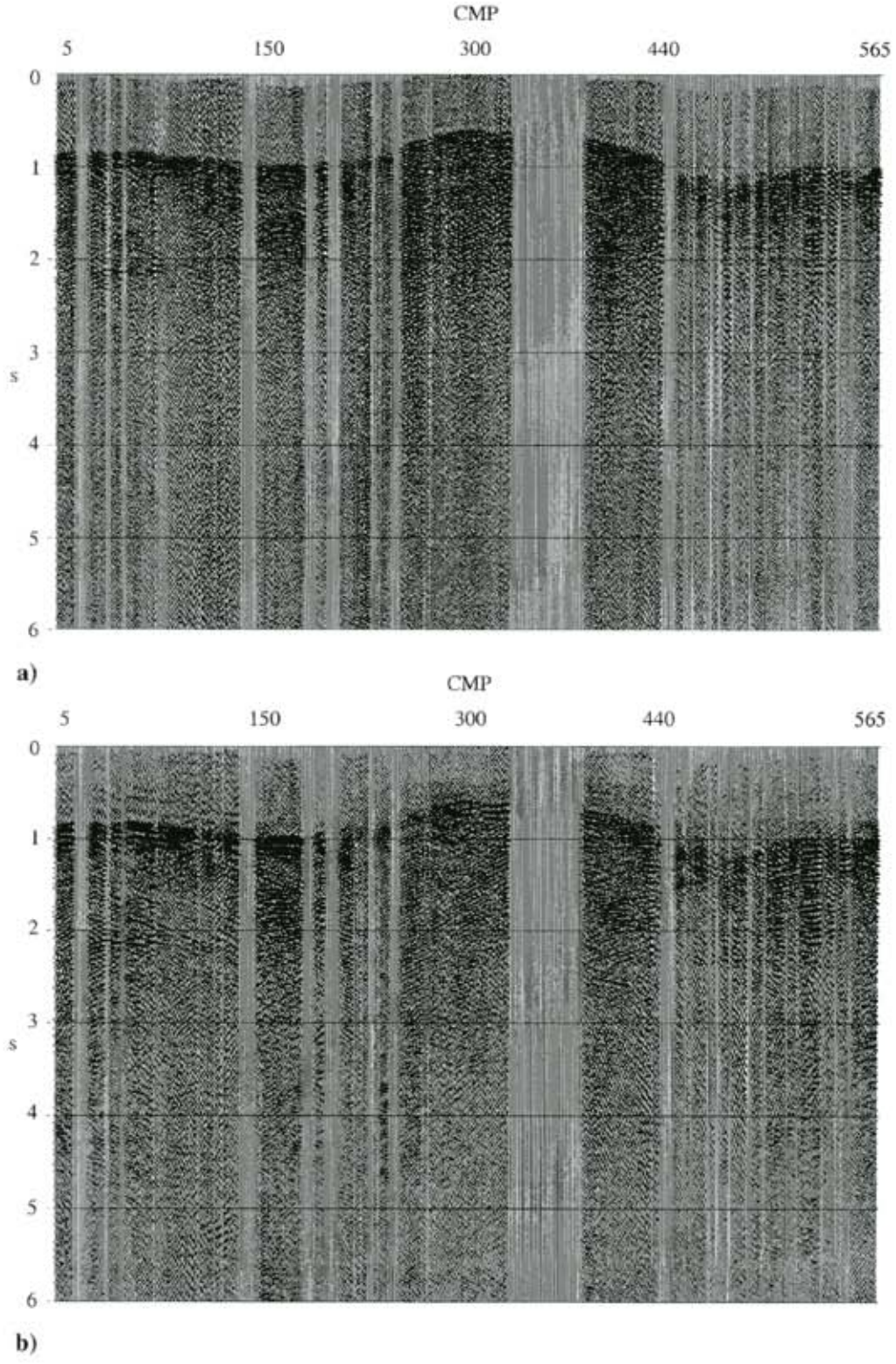

FIG. 10. Common-offset (3000 m) gather relative to the western area (CMPs 5–565) with static corrections to the flat datum (a) before and (b) after *f-x* deconvolution.

model is estimated through in-house developed codes based on the WIM (Zanzi, 1996) and GRM (Palmer, 1980) methods. GRM was applied on explosive shots integrated with an appropriate selection of Vibroseis records where explosive-source data were too sparse. The phase matching of the explosive and Vibroseis data was accomplished by calibrating the picking procedure at locations where both sources had been used. Where the first arrivals of the forward and reverse dynamite shots did not overlap sufficiently, the WIM method was applied on Vibroseis data and the results were merged. Statics were calculated to a floating datum designed by smoothing the topography. A variable replacement velocity was used to account for the rapid lateral variations of the near-surface lithology. A lesson we learned is that the design of the floating datum should be calibrated with the spread extension length. In this specific case, given the rather long spread, a heavy smoothing of the topography was needed to define a suitable floating datum. The final (flat) datum was set at an elevation of 400 m above sea level, which is the average elevation of the profile, resulting in a static range from −200 to +100 ms. (For an example of the static trend, see the elevation and static profiles at the top of Figure 16.)

The correspondence between the refractor velocity variation and the changes in the shallow lithology is noticeable (Figure 3). Also note that the repetition of lithological units along the line nicely matches the refractor velocity values (e.g., the segments indicated by *c*, the terrigenous deposits, and *d*, the Alburno–Cervati carbonates). This characteristic helped determine the optimal static corrections for the Monte Soprano area. In this zone, where the shot repetition rate is very low because of accessibility problems, the refractor velocities directly estimated from the first breaks (dotted line, Figure 3) are unreliable and are not comparable with those obtained for the same lithology in other parts of the line (4000–4500 m/s). Thus, for this specific section, static corrections were determined by trial and error and by visually inspecting the results. Each static computation test was conducted using a different refractor velocity, including those pertaining to the same lithology along the line.

The good correlation between the refractor-derived model and the geological elements indicates good reliability in our refractor velocity estimates. In addition, the effectiveness of the datum static corrections we applied is evident on comparing the constant-velocity stacks before and after application (Figure 12).

Residual time shifts were further corrected by means of surface-consistent residual statics computed on NMO-corrected CMP gathers. These were calculated along time gates centered on the major seismic events, with a temporal width >1 s. In general, we imposed at least three time gates for each CMP location and let the algorithm search for the solution that simultaneously maximized the power of the stack of all the time windows considered. The maximum allowed time shift at each station was 30 ms.

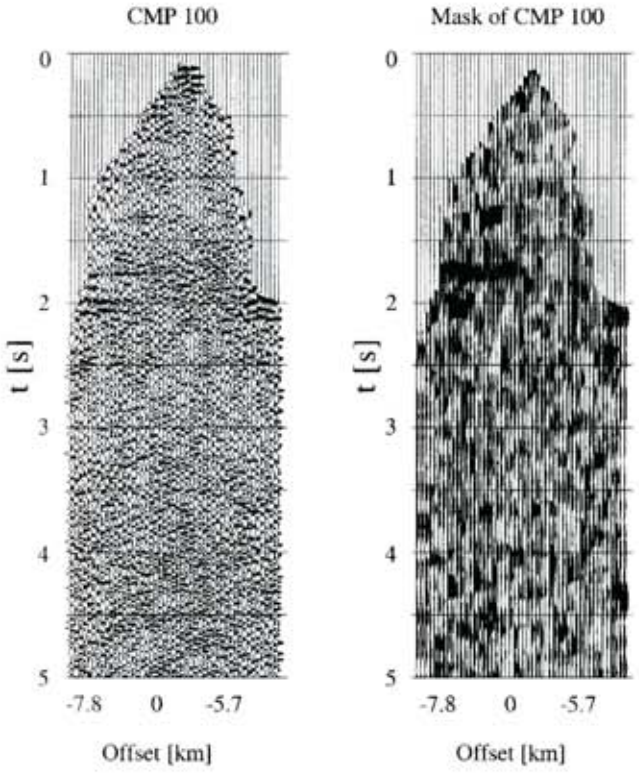

FIG. 11. NMO-corrected CMP gather with residual statics applied (left) and corresponding stacking weights (right) computed by means of crosscorrelation. The value of the weights is given by the excursion of the wavelets. Highest weights are located along coherent reflections. Poor data-quality zones are highlighted by corresponding low-amplitude weights.

Optimization of CMP sorting

The high tortuosity of the line significantly degrades the stack quality, especially for the shallow reflections. To limit this negative effect as much as possible, we tested three different criteria for CMP sorting, as illustrated in Figure 13. Minimum curvature, the method used in the previous processing sequence, favors the CMP distribution that minimizes the curvature of the line. Results of this sorting procedure are shown in Figure 13a, where we present a supergather that is the sum of five adjacent CMPs in the area between the Albanella and Alburno Mountains (CMP 617). With maximum density, the line follows the zones of the profile where the CMPs are more densely spaced. Figure 13b illustrates the results of this CMP gathering with the same supergather. Finally, in short offsets the resulting line follows a path through the zones more densely populated by CMPs composed of traces with source–receiver offset up to a given value. Figure 13c shows the results of this technique up to a maximum offset of ±2.5 km (about one-fourth of the spread).

Figure 13 reveals that the short-offset method yields the optimum S/N results. In fact, with this method the shapes of the reflections are more distinguishable and approach a quasi-hyperbolic move-out (e.g., the reflections at 0.6–0.8 s). The same observations were reached on examining the results in other segments of the line. Only in limited segments of the line, between CMPs 1271–1390 and 1470–1490, did the maximum density criterion produce the best results. Thus, with the exception of these two segments where we used the maximum density method, we gathered all the CMPs of the line following the short-offset criterion.

Model-driven velocity analysis

Also, the determination of the optimal stacking velocity field required much manpower. Although the quality of the data at

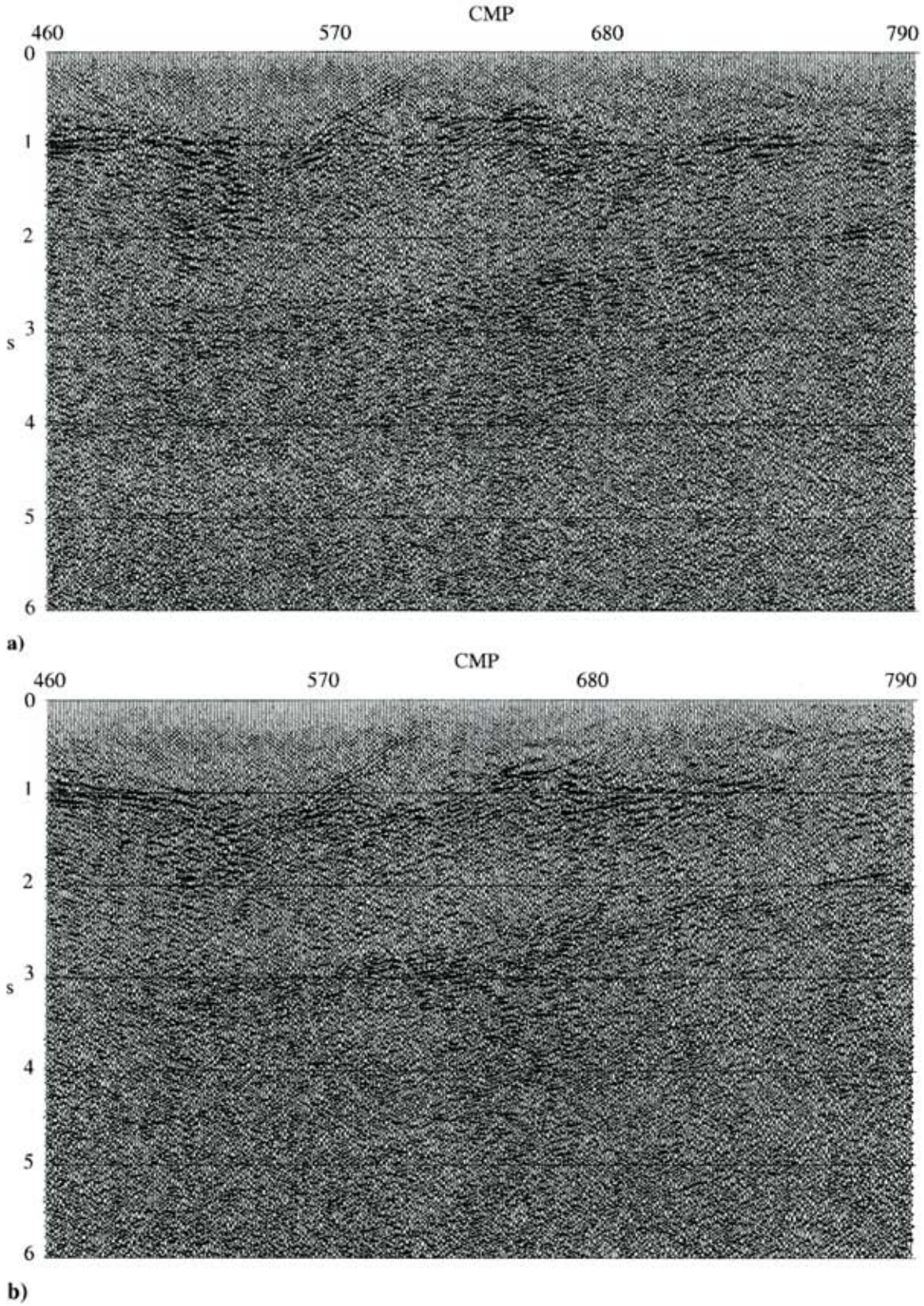

FIG. 12. Static correction results: (a) CVS (5500 m/s) in the area between the Albanella and Alburno Mountains before appliying the static corrections; (b) the same CVS as in (a) but with the statics to the final datum (400 m above sea level) applied.

this phase was considerably improved with respect to the original data, there were still areas where the velocity picking was difficult. The lateral surface velocity variation and the low S/N ratio prompted us to proceed with a global preliminary analysis of the velocity field. Constant-velocity stacks (CVS) for the whole line with velocity intervals of 250 to 500 m/s were produced and carefully studied to determine the initial velocity field. This was then refined on CMP velocity spectra for a more detailed definition. The resulting stack was compared with the CVS, and the procedure was iterated until the result was considered satisfactory. Even the slightest evidence of lateral coherence that appeared or disappeared during these iterations was discussed with interpreters and compared with the available geological data of the area. In some part of the line, the geological data (outcrops, published borehole data) made it possible to define plausible models of the subsurface that were used as soft constraints to guide the velocity analysis. A further revision of the velocity field using velocity spectra analysis was also performed after the residual statics application.

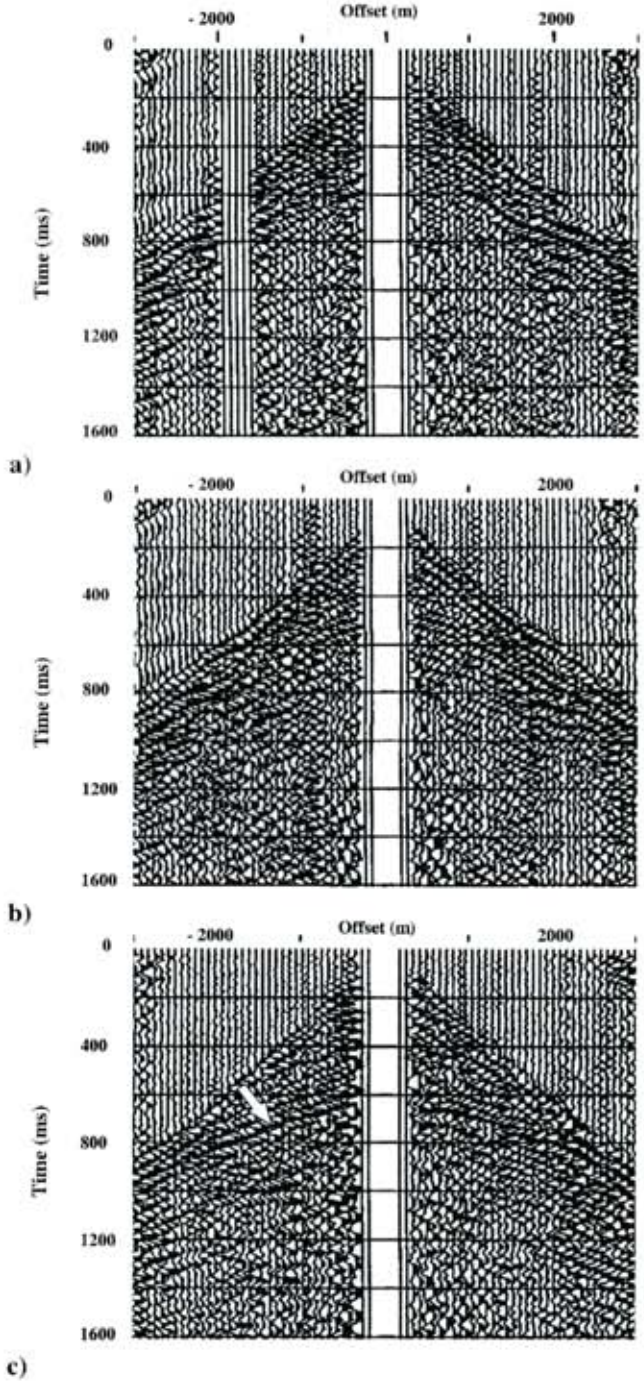

FIG. 13. Results from the optimization of the CMP gathering. Three different gathering criteria are compared on a super CMP (sum of five adjacent CMPs): (a) minimum curvature (applied in the previous processing sequence); (b) maximum density; and (c) short offsets. The white arrow points to the reflections that become particularly evident when the short-offset criterion is used.

DISCUSSION OF THE RESULTS

Our final results in terms of stacked time section are compared with the outcome of a processing sequence that had already been applied. Table 2 shows this standard sequence. It differs from the one we propose in many aspects:

1) there was no measurement-based removal of low-quality traces;
2) the refraction statics were computed directly to the flat datum and with a constant replacement velocity, while the picking of first breaks was performed on vibroseis data only;
3) the CMP sorting was carried out using the less effective minimum curvature method; and
4) attempts to enhance the coherency of the data involved CMP-consistent residual statics (trim statics) and post-stack dip enhancement techniques.

Table 2. Standard processing sequence applied to the CROP 04 line.

AGC	(windows: 256–2048 ms)
Refraction Statics	(single refractor, constant replacement velocity, flat datum, 400 m above sea level)
Array Simulation	(five traces, Chebyshev weights: 0.164, 0.584, 1, 0.584, 0.164)
Predictive Deconvolution	
windows:	1-from 0.0 to 3.0 s 2-from 3.0 to 10.0 s
prediction distance	56 ms
operator length	300 ms
white light	1%
Sorting to CMP Gathers	(minimum curvature criterion)
Velocity analysis	
velocity increment	100 m/s
NMO	
CMP-Consistent Residual Statics	
traces	3
windows:	1-from 0.0 to 6.0 s 2-from 6.0 to 12.0 s
maximum shift	24 ms
Stack	
Radial Predictive Filter	(19 traces)
Time-Variant Filter	

time (s)	L.C. (Hz, DB/OCT)	H.C.
1.0	9/24	45/48
3.0	8/24	40/48
6.0	7/24	35/48
25.0	6/24	30/48

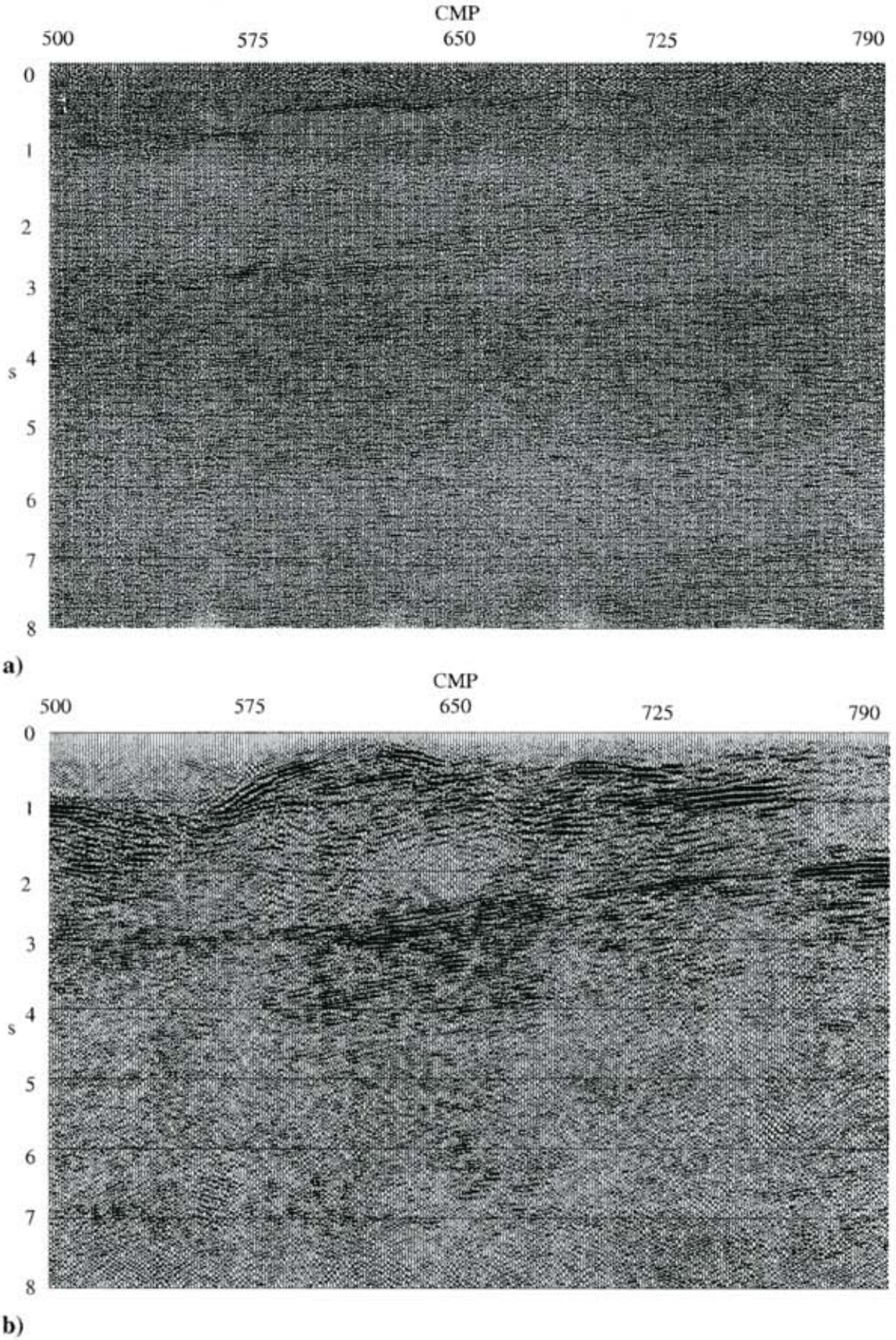

FIG. 14. Comparison of the final results in the Controne area: (a) final stack section from the previous processing sequence; (b) final stack section with the sequence used in this work.

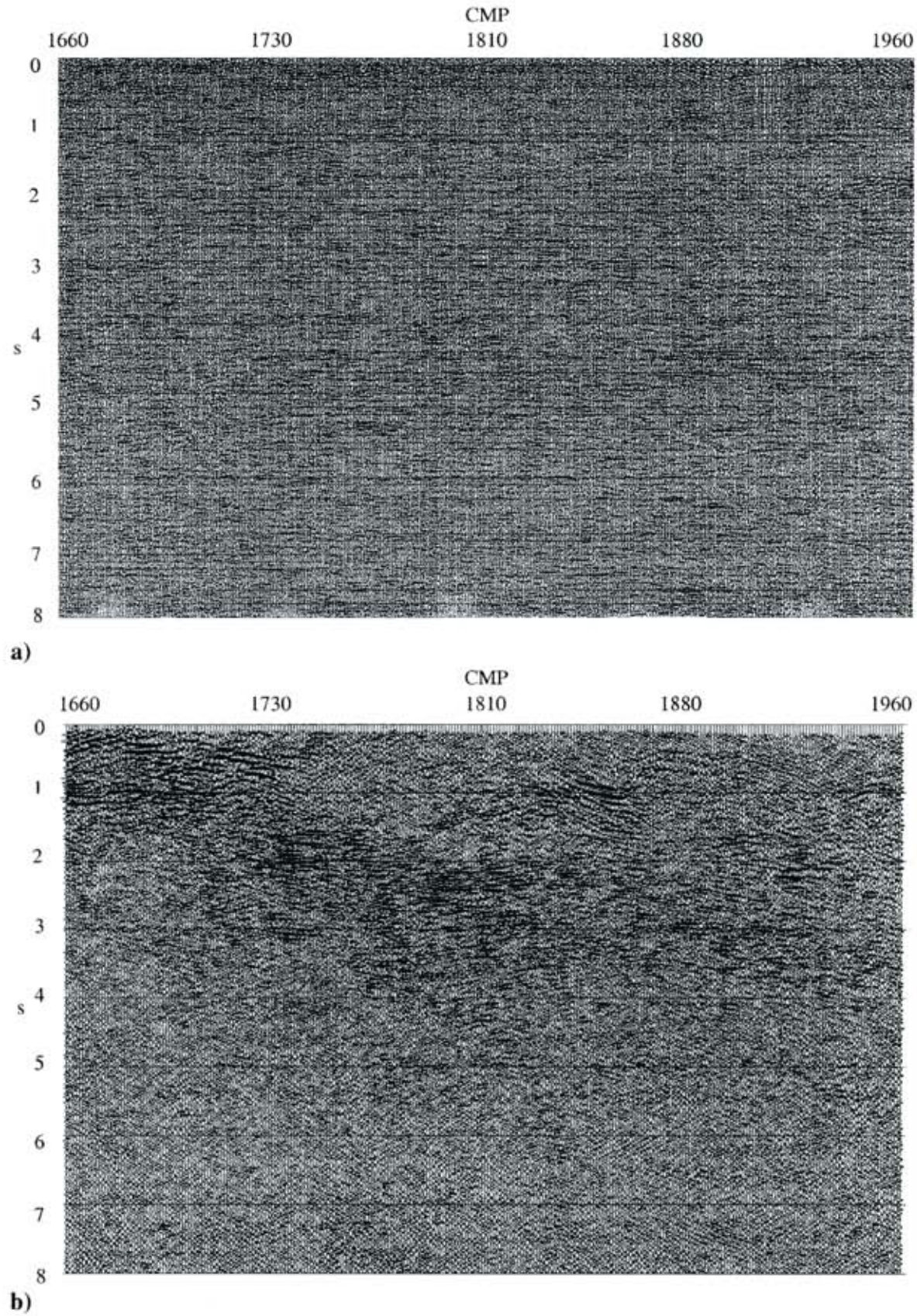

FIG. 15. Comparison of the final results in the San Fele area: (a) final stack section from the previous processing sequence; (b) final stack section produced with the sequence used in this work.

Thus, apart from the array simulation filter, there was no early attempt to remove the large amount of noise affecting the data, and the statics and CMP sorting were performed differently. Attempts to recover some coherence in the data were made in extremis by means of poststack coherency enhancement techniques.

We present the comparison between the results of the two processing sequences in two areas of the whole profile. One is located at the beginning of the line, between CMPs 500 and 790, close to the Controne area. The new stack section of this area has continuous and structured events at times down to 8 s (Figure 14b); such events were not clearly discernible in the previous version (Figure 14a). Depending on the interpretation, these reflectors may be related to the Moho discontinuity or to very deep sedimentary layers. The other area, close to the San Fele area (CMPs 1720–1960), cuts across a thick antiformal stack of Lagonegro imbricates within the roof units of the duplex system (San Fele antiform). This is the most difficult segment of the profile and, as shown in Figure 15a, originally had a very low useful seismic reflection response. This has been clearly improved, and the final stack now presents many events (at least in the upper part of the section) down to 4 s (Figure 15b).

The new processing sequence produced similar improvements in the other segments of the line. Great care was taken in checking the reliability of the results. In fact, since the quality of the raw field data was so poor, we were constantly worried about the possibility of creating false events by introducing processing artifacts or by enhancing a particular kind of noise. To avoid this most unwanted outcome, we checked the result of each processing step to verify that nothing extraordinary had happened and that the intermediate results were in accordance with the plausible geological models of the area. Also, where possible, surface-consistent operations were applied, and no attempt was made to artificially or overly force the data coherency. Finally, the multichannel operations that are designed to attenuate random noise and that implicitly improve the continuity of reflections, e.g., f-x deconvolution, were carried out after a careful choice of the parameters.

As far as quality is concerned, the reprocessed seismic section is comparable with the best commercial lines in the region.

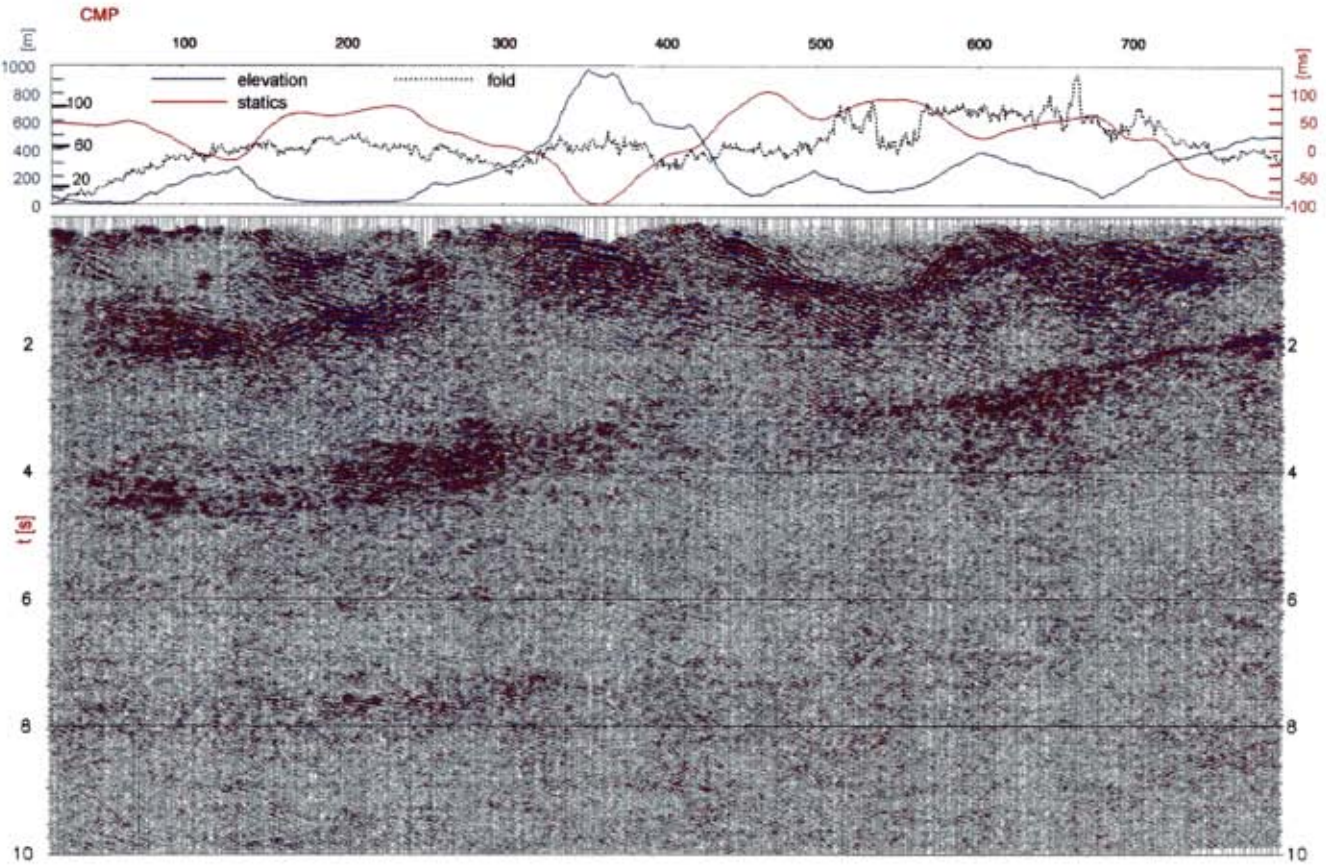

FIG. 16. Final stack of the western segment of the profile (from CMPs 5 to 790). The graphs for elevation, statics to the final datum, and stack fold are also shown. The reflection-free body between 2 and 4 s at the left end of the section and between 0 and 2 s at the right end corresponds to a thick sequence (>5000 m) of shallow-water Mesozoic–Tertiary carbonates (Alburno-Cervati unit) tectonically overlain (see two marked synforms) by the Sicilide nappe and by the thrust-sheet-top deposits unconformably covering the Ligurian Nappe. The package of strong reflectors which deepens from 2 s (right end) to 4 s (left end) has been interpreted in Figure 2 as a stack of basinal deposits sandwiched between the Alburno-Cervati nappe and the buried duplex system of Apulia carbonates. Note the package of northeast-climbing faint reflectors in the right side of the section between 6 and 8 s; the geological interpretation of these reflectors (tectonic structures involved in the orogenic transport according to our interpretation) has strongly influenced the overall geometrical reconstruction of the thrust belt sketched in Figure 2.

Nevertheless, records suitable for interpretation do not usually exceed 5–6 s in commercial lines, while continuous and well-structured events are recognizable in the new stack section down to 8 s (see Figure 16). This difference is substantial for fixing the depth of the sole-thrust and for constructing a balanced geological section. Figure 2 is asimplified cross-section derived from a preliminary interpretation of the seismic section. A key point is represented by the presence of a well-organized package of reflectors beneath the Alburno Mountains at a depth of 6–8 s (see right end of the section in Figure 16). The geometry of these reflectors suggests a very deep (20–25 km) sole-thrust of the Apenninic chain in the area. Ongoing work, including horizon depth migration and section balancing, is being addressed to better understand the real geometry and the geological meaning of these events.

CONCLUSIONS

The organization of this project in two distinct phases of data analysis and data processing, though requiring a significant amount of both manpower and CPU time, has been the basis for the successful improvement of the data quality. Another key factor has been the constant interaction between geophysicists, responsible for reprocessing the data, and geologists with an accurate geologic knowledge of the area. This cooperation has been particularly fruitful in the data analysis phase, in checking the consistency of the refractor velocities with surface geology, and in the velocity analysis/interpretation.

No single phase of this processing sequence can be considered the key to the success of this project. Rather, the whole process produced a significant improvement in the final results. The project took about one year and was carried out by a team that included senior geophysicists and geologists and two full-time research fellows. The most time-demanding phases of the project were the preliminary analysis of the data quality, the statics computation, and the velocity analysis.

This work has not only improved the quality and interpretability of this specific data set, but its results may also serve as the basis for the future acquisition and processing of seismic data in nearby areas or in regions with similar characteristics.

ACKNOWLEDGMENTS

This work was supported by the CROP project. We thank the sponsoring institutions of the project—CNR, ENI/AGIP, and ENEL—for permission to publish these results. We gratefully acknowledge the continuous support of M. Bernabini (CNR), L. Bertelli (ENI/AGIP), and S. D'Offizi (ENEL). Thanks are given to A. Morgante of ENEL for his contribution in the geological models. The seismic processing was carried out using ProMAX software from Landmark Graphics Corp. The codes for static corrections, weighted stacking, and trace quality analysis were developed internally.

REFERENCES

Balduzzi, A., Casnedi, R., Crescenti, U., Mostardini, F., and Tonna, M., 1982a, Il Plio-Pleistocene del sottosuolo del Bacino Lucano (Avanfossa Appenninica): Geol. Romana, **21**, 89–111.

Balduzzi, A., Casnedi, R., Crescenti, U., and Tonna, M., 1982b, Il Plio-Pleistocene del sottosuolo del Bacino Pugliese (Avanfossa Appenninica): Geol. Romana, **21**, 1–28.

Casero, P., Roure, F., and Vially, R., 1991, Tectonic framework and petroleum potential of the southern Apennines, *in* Spencer, A. M., Ed., Generation, accumulation, and production of Europe's hydrocarbons: Eur. Ass. Petr. Geosci. Special Publ., **1**, 381–387.

Casnedi, R., 1988a. La fossa bradanica: Origine, sedimentazione e migrazione: Mem. Soc. Geol. Italiana, **41**, 439–448.

———1988b. Subsurface basin analysis of fault-controlled turbidite system in Bradano trough, southern Adriatic foredeep, Italy: AAPG Bulletin, **72**, No. 11, 1370–1380.

D'Andrea, S., Pasi, R., Bertozzi, G., and Dattilo, P., 1993, Geological model, advanced methods help unlock oil in Italy's Apennines: Oil & Gas J., August 23, 53–57.

Grion, S., and Mazzotti, A., 1998, Stacking weights determination by means of SVD and cross-correlation: 68th Ann. Internat. Mtg., Soc. Expl. Geophys., Expanded Abstracts, 1135–1138.

La Bella, G., Bertelli, L., and Savini, L., 1996, Monte Alpi 3D: A challenging 3D survey in the Apennine Range, southern Italy: First Break, **14**, 285–294.

Mattavelli, L., Pieri, M., and Groppi, G., 1993, Petroleum exploration in Italy: A review: Marine Petr. Geol., **10**, 410–425.

Mostardini, F., and Merlini, S., 1986, Appennino centro-meridionale: Sezioni geologiche e proposta di modello strutturale: Mem. Soc. Geol. Italiana, **35**, 177–202.

Palmer, D., 1980, The generalized reciprocal method of seismic refraction interpretation: Soc. Expl. Geophys.

Roure, F., and Sassi, W., 1995, Kinematics of deformation and petroleum system appraisal in Neogene foreland fold-and-thrust belts: Petr. Geol., **1**, 253–269.

Sella, M., Turci, C., and Riva, A., 1988, Sintesi geopetrolifera della Fossa Bradanica (avanfossa della catena appenninica): Mem. Soc. Geol. Italiana, **41**, 87–107.

Wu, W. J., Lines, L., Burton, A., Lu, H. X., Zhu, J., Jamison, W., and Bording, R. P., 1998, Prestack depth migration of an Alberta Foothills data set—The Husky experience: Geophysics, **63**, 392–398.

Zanzi, L., 1996, The WIM method for refraction statics: Geophysics, **61**, 1859–1870.

Zhu, X., Angstman, B. G., and Sixta, D. P., 1998, Overthrust imaging with tomo-datuming: A case study: Geophysics, **63**, 25–38.